Invited Paper

Computational methods for image restoration, image segmentation, and texture modeling

Ginmo Chung, Triet M. Le, Linh H. Lieu, Nicolay M. Tanushev and Luminita A. Vese

University of California, Los Angeles, Department of Mathematics,
405 Hilgard Avenue, Los Angeles, CA 90095-1555, U.S.A.

ABSTRACT

This work is devoted to new computational models for image segmentation, image restoration and image decomposition. In particular, we partition an image into piecewise-constant regions using energy minimization and curve evolution approaches. Applications of denoising-segmentation in polar coordinates (motivated by impedance tomography) and of segmentation of brain images will be presented. Also, we decompose a natural image into a cartoon or geometric component and an oscillatory or texture component using a variational approach and dual functionals. Thus, new computational methods will be presented for denoising, deblurring and texture modeling.

Keywords: Computational imaging, functional minimization, P.D.E., decomposition, denoising, segmentation

1. INTRODUCTION

In this paper we present several models and computational imaging results that will illustrate the use of functional minimization and of Euler-Lagrange equations for different but related image processing tasks: image restoration, image decomposition into cartoon and texture, and image segmentation. The proposed techniques can be seen as refinements or variants of previous canonical models (the Mumford and Shah model[1] for image segmentation and the total variation minimization of Rudin-Osher-Fatemi for image restoration[2]). Our segmentation models can also be seen as extensions of the active contour models without edges introduced in,[3] ,[4] ,[5] .[6] Applications to brain MRI image segmentation and to processing of images in polar coordinates, motivated by impedance tomography, will be presented.

We first give our main notations and motivations. Let Ω be an open and bounded domain in $\mathbb{R}^n$ and let $f : \Omega \to \mathbb{R}$ be a given image. In particular we consider here the case of planar images ($n = 2$) and of volumetric images ($n = 3$). The case of vector-valued data could be considered as well. Often the observed data f is a noisy and blurry version of an original image u that has to be extracted from f. This is in general an inverse ill posed problem, and additional assumptions on u and on the degradation model are needed. Sometimes we would like u to be a piecewise-smooth approximation of f; therefore u is formed by homogeneous regions and with sharp edges (called a cartoon, geometric or simplified version of f). Additive (or multiplicative) details like noise and texture (oscillatory patterns) are not kept in u; these remain in the residual term $f - u$ (or $\frac{f}{u}$ respectively for multiplicative noise). A related problem is to extract a piecewise-smooth approximation to f and the edges between these smooth regions. This problem is referred to as segmentation or partition of f.

One of the most well known methods for image segmentation or partition is the one formulated by Mumford and Shah. We recall here the piecewise-constant case, or the minimal partition problem,[1] where an image f is

Further author information: (Send correspondence to L.A.V.)
G.C.: E-mail: senninha@math.ucla.edu
T.M.L.: E-mail: tle@math.ucla.edu
L.H.L.: E-mail: llieu@math.ucla.edu
N.M.T.: E-mail: nicktan@math.ucla.edu
L.A.V.: E-mail: lvese@math.ucla.edu

Computational Imaging IV, edited by Charles A. Bouman, Eric L. Miller, Ilya Pollak,
Proc. of SPIE-IS&T Electronic Imaging, SPIE Vol. 6065, 60650J, © 2006 SPIE-IS&T · 0277-786X/06/$15

partitioned into several regions Ω_i, and the gray-scale level in each Ω_i is close to an average constant c_i. This can be accomplished by minimizing the following energy functional[1]:

$$E^{MS}(u, C) = \lambda \sum_i \int_{\Omega_i} |f(x) - c_i|^2 dx + \mu \text{ length}(C), \tag{1}$$

where μ and λ are tuning parameters, C is a piecewise smooth curve that partitions Ω into Ω_i, and $u = c_i$ is constant in each Ω_i. A simple observation shows that for a fixed C, the value of c_i that minimizes this functional is given by the average of f over Ω_i. This model can be used for image denoising as well as segmentation. If the image is noisy, but the original true image is piecewise constant, then this minimization will lead to a partition and will give the average value of f in each region. Thus, the segmented image u will give a denoised version of f. However in practice, it is difficult to minimize the functional. Solutions have been proposed by the elliptic approximations of Ambrosio and Tortorelli,[7] ,[8] by the region growing and merging method of Koepfler, Lopez and Morel,[9] and more recently by the use of curve evolution and of implicit representation in Chan and Vese,[3] ,[4] ,[5] ,[6] Tsai, Yezzi, Willsky,[10] among other work.

The Mumford and Shah minimization problem can be put in the level set framework in the following way. Suppose first that we are working in the simplified case of binary segmentation. The image f can be partitioned using a level set function ϕ into two regions, one region where $\phi > 0$ and another where $\phi < 0$. The zero level set of ϕ will define the curve C. Its length will be given by $\int |\nabla H(\phi)| dx = \int \delta(\phi) |\nabla \phi| dx$, where H is the Heaviside function and δ is the Dirac delta function. In this case, the functional (1) can be rewritten as,[3] [4]

$$E_2^{CV}(c_1, c_2, \phi) = \lambda \int_\Omega \Big[|f(x) - c_1|^2 H(\phi(x)) + |f(x) - c_2|^2 (1 - H(\phi(x))) \Big] dx + \mu \int_\Omega \delta(\phi) |\nabla \phi| dx. \tag{2}$$

We use here the variational level set approach introduced in Zhao, Chan, Merriman, and Osher.[11] Following the observation from the previous paragraph, the optimal constants c_1 and c_2 for a fixed ϕ are given by

$$c_1 = \frac{\int_\Omega f(x) H(\phi(x)) dx}{\int_\Omega H(\phi(x)) dx} \qquad \text{and} \qquad c_2 = \frac{\int_\Omega f(x)(1 - H(\phi(x))) dx}{\int_\Omega (1 - H(\phi(x))) dx}. \tag{3}$$

Introducing an artificial time, $t \geq 0$, one verifies that with $\phi(x, t)$ satisfying

$$\frac{\partial \phi}{\partial t} = \delta(\phi) \Big[\mu \nabla \cdot \frac{\nabla \phi}{|\nabla \phi|} - \lambda |f - c_1|^2 + \lambda |f - c_2|^2 \Big] \quad \text{in} \quad \Omega \tag{4}$$

$$\frac{\partial \phi}{\partial \nu} = 0 \quad \text{on} \quad \partial\Omega, \tag{5}$$

E_2^{CV} will be a non-increasing function of t (here ν denotes the exterior unit normal to $\partial\Omega$).

The level set formulation of segmentation is not limited to binary segmentation. One way to extend the model is to use n level set functions that can partition an image into 2^n regions, as introduced in.[6] Each region is determined by the signs of the level set functions. The extension to multiple level set functions follows immediately from the previous section. As an example we discuss the case of two level set functions, ϕ and ψ. These functions define four disjoint regions, $\{\phi > 0, \psi > 0\}$, $\{\phi > 0, \psi < 0\}$, $\{\phi < 0, \psi > 0\}$, and $\{\phi < 0, \psi < 0\}$. The four-phase Chan-Vese model (as a modified Mumford and Shah functional) is analogously given by

$$\begin{aligned} E_4^{CV}(c_1, c_2, c_3, c_4, \phi, \psi) &= \lambda \int_\Omega \Big[|f(x) - c_1|^2 H(\phi(x)) H(\psi(x)) + |f(x) - c_2|^2 H(\phi(x))(1 - H(\psi(x))) \\ &+ |f(x) - c_3|^2 (1 - H(\phi(x))) H(\psi(x)) + |f(x) - c_4|^2 (1 - H(\phi(x)))(1 - H(\psi(x))) \Big] dx \\ &+ \mu \int_\Omega \Big[\delta(\phi) |\nabla \phi| + \delta(\psi) |\nabla \psi| \Big] dx, \end{aligned}$$

where the union of curves C is now defined by $C = \{x \in \Omega : \ \phi(x) = 0\} \cup \{x \in \Omega : \ \psi(x) = 0\}$. For fixed ϕ and ψ, the coefficients, c_1, c_2, c_3 and c_4, that minimize E_4^{CV} are given by the average of f over each one of these

regions. We note that in the energy E_4^{CV}, overlapping pieces of contours of $\{\phi = 0\}$ and of $\{\psi = 0\}$ may count more than once in the length term. This can be avoided by a minor modification.

The equations for ϕ and ψ are a direct analog of equation (4),

$$\begin{aligned}
\frac{\partial \phi}{\partial t} &= \delta(\phi)\Big[\mu\nabla\cdot\frac{\nabla\phi}{|\nabla\phi|} - \lambda\big[|f-c_1|^2 - |f-c_2|^2\big]H(\psi) - \lambda\big[|f-c_3|^2 - |f-c_4|^2\big]\big(1-H(\psi)\big)\Big] \\
\frac{\partial \psi}{\partial t} &= \delta(\psi)\Big[\mu\nabla\cdot\frac{\nabla\psi}{|\nabla\psi|} - \lambda\big[|f-c_1|^2 - |f-c_3|^2\big]H(\phi) - \lambda\big[|f-c_2|^2 - |f-c_4|^2\big]\big(1-H(\phi)\big)\Big],
\end{aligned}$$

with similar Neumann boundary conditions on $\partial\Omega$.

Numerically, for the Heaviside and Dirac delta functions, we use the approximations,[3 4]

$$H_\epsilon(x) = \frac{1}{2}\Big[1 + \frac{2}{\pi}\arctan\Big(\frac{x}{\epsilon}\Big)\Big] \qquad \text{and} \qquad \delta_\epsilon(x) = H_\epsilon'(x) = \frac{1}{\pi}\frac{\epsilon}{\epsilon^2 + x^2}. \tag{6}$$

The above two segmentation models using curve evolution will be applied in the next section to images defined on circular domains.

One of the standard methods for denoising and deblurring images is the Rudin-Osher-Fatemi model,[2] .[12] In their model, these two tasks are carried out by minimizing the energy functional,

$$E^{ROF}(u) = \int_\Omega |\nabla u| dx + \lambda \int_\Omega |f - Ku|^2 dx, \tag{7}$$

over functions u of bounded variation $\int_\Omega |\nabla u| dx < \infty$. The first term ensures that u is not rapidly oscillating but preserves edges, while the second term keeps Ku close to the original image f (based on the linear degradation model assumption "$f = Ku+$ white Gaussian noise"). Respectively, these two terms are referred to as the regularizing term and the fidelity term. The blur operator K is linear and continuous from $L^2(\Omega)$ to $L^2(\Omega)$ and is in general a convolution or the identity. The tuning parameter λ balances these two quantities against each other. To solve this convex minimization, it is again convenient to introduce an artificial time parameter $t \geq 0$. By letting u depend on t through the equation

$$\frac{\partial u}{\partial t} = \nabla\cdot\frac{\nabla u}{|\nabla u|} + 2\lambda K^*(f - Ku) \quad \text{in} \quad \Omega \tag{8}$$

$$\frac{\partial u}{\partial \nu} = 0 \quad \text{on} \quad \partial\Omega\,, \tag{9}$$

one can easily verify that E^{ROF} will be a non-increasing function of t. Thus, we expect that as $t \to \infty$, $u(t)$ will give us a minimum of E^{ROF}. Here, K^* denotes the adjoint operator of K. This model will be applied in the next section to denoising of images defined on circular domains ($K = I$), while in Section 4, the model will be further refined.

The outline of the paper is as follows. In Section 2 we show computational results of image denoising and segmentation when the data is given in polar coordinates. In Section 3 we segment 3D MRI data into three anatomical regions, using the multilayer level set approach, while in Section 4, the last section of the paper, we propose image decomposition models based on duality, together with experimental results for denoising and deblurring.

2. DENOISING AND SEGMENTATION MODELS IN POLAR COORDINATES

In this section we present some results on denoising and segmentation in polar coordinates. This study was motivated by a problem in electrical impedance tomography in which data was gathered on a circular boundary. In that setting, it was most natural to consider the problem of image segmentation in polar coordinates. The formulations of the R-O-F[2] and the C-V models,[4 6] in polar coordinates are identical to their formulations in

Cartesian coordinates, except for the boundary conditions and the form of the divergence operator. In polar coordinates (r, θ) with $0 \leq r \leq 1$, $0 \leq \theta < 2\pi$ we have

$$\nabla = \left(\frac{\partial}{\partial r}, \frac{1}{r} \frac{\partial}{\partial \theta} \right). \tag{10}$$

The most natural boundary conditions are periodic boundary conditions in $\theta \in [0, 2\pi)$, Neumann boundary condition at the edge of the circle $r = 1$ and continuity at the origin $r = 0$.

In what follows, we will consider a unit circle, Ω, and an image given by a function $f : \Omega \to I\!R$. The denoised or segmented version of the image will be denoted by u.

2.1. TV Denoising in Polar Coordinates

To avoid dividing by 0 at the origin in equation (8), we multiply $\frac{\nabla u}{|\nabla u|}$ by $\frac{r}{r}$ and use the standard regularization of adding a small positive number ϵ to the denominator. We apply periodic boundary conditions in θ and Neumann boundary conditions at $r = 1$. At the origin, we define u to be the average of its values at $r = \triangle r$. Results for denoising two synthetic images with additive noise are shown in Figure 1 and in Figure 2. In both cases, the initial condition is $u(0) = f$.

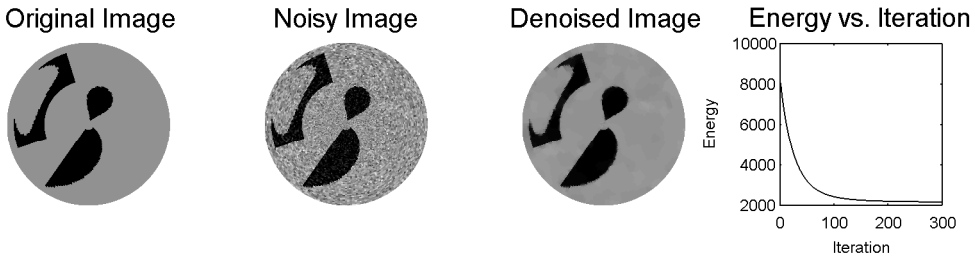

Figure 1. Results for denoising a synthetic noisy image using the ROF model in polar coordinates. The original binary image is degraded by additive zero-mean Gaussian noise with standard deviation of 20 and RMSE=19.9158 (root mean square error, normalized). The tuning parameter λ equals 1. The denoised image has the RMSE=5.2919.

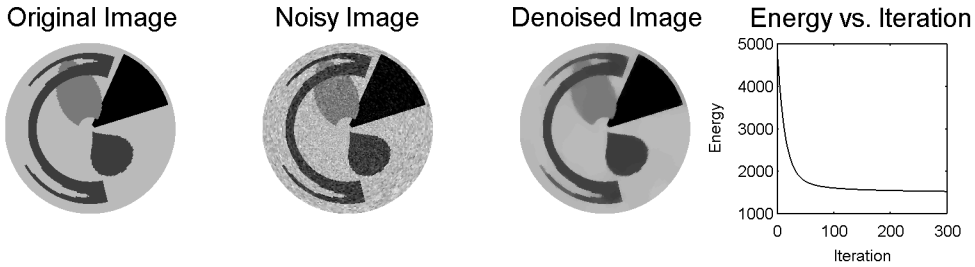

Figure 2. Results for denoising another synthetic noisy image using the ROF model. The original four-phase image is degraded by additive zero-mean Gaussian noise with standard deviation of 10 and RMSE=9.9158. The tuning parameter λ equals 1. The denoised image has the RMSE=4.7138.

2.2. Segmentation in Polar Coordinates

In this subsection we show how the C-V segmentation models can be used for piecewise-constant segmentation of data given in polar coordinates, as in impedance tomography.

2.2.1. Two-Phase Segmentation in Polar Coordinates

To solve equation (4) that results from the C-V binary segmentation model in polar coordinates, we employ a semi-implicit discretization in space and a variable step size algorithm in time. The time step is increased or decreased between a maximum and a minimum value based on how quickly the coefficients c_1 and c_2 are changing. This allows for a very small time step initially, when ϕ and the constants are evolving rapidly, while still maintaining reasonable computational times for the segmentation.

Figure 3 shows the segmentation of a binary image that has been degraded with additive Gaussian noise. The segmentation in this case leads to the exact reconstruction of the original true image. Similar numerical results are obtained for a large variety of initial conditions.

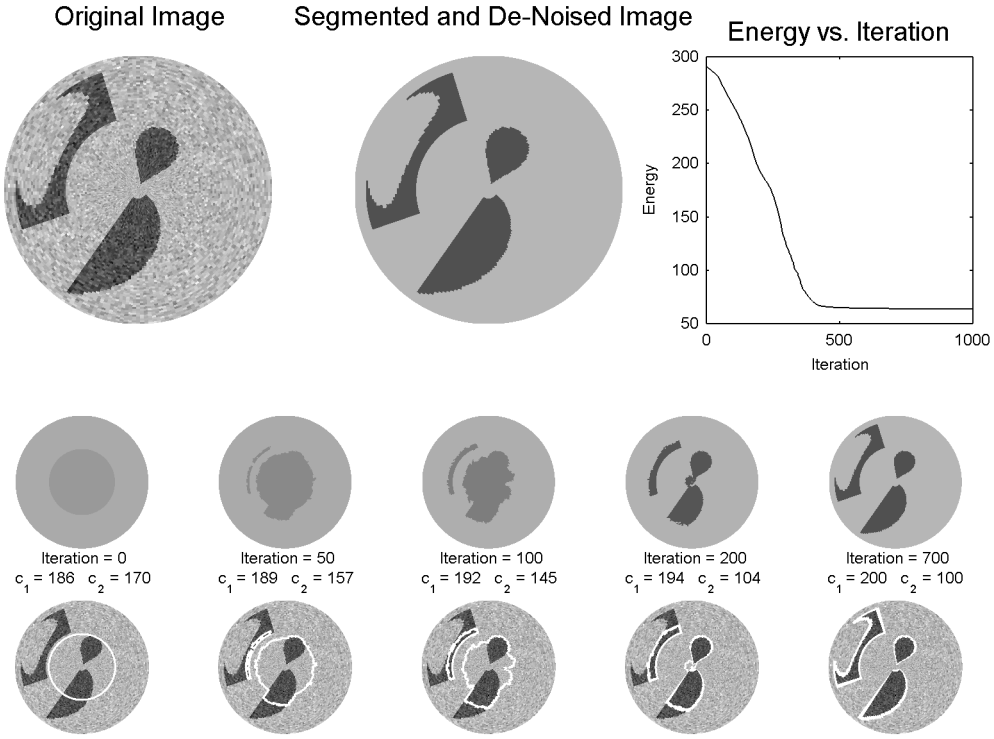

Figure 3. Segmentation using a single level set function. The original two color image is degraded by additive zero-mean Gaussian noise with standard deviation of 20 and RMSE=19.9158. The values for c_1 and c_2 in the original clean image are 100 and 200. In this example $\lambda = .05$ and $\mu = 1$. The two regions and the values of constants are recovered perfectly (with RMSE=0.9005 for the denoised image). The bottom five pairs of images show the evolution of the level set function as well as the values of the coefficients at the given iteration.

2.2.2. Four-Phase Segmentation in Polar Coordinates

Numerical results for a four-phase segmentation of a synthetic noisy image are given in Figure 4. The segmentation is very accurate, except for some minor errors in the upper part of the image. In this case, we remark that the segmentation result depends more strongly on the initial choice for level set functions than the binary segmentation case. There is numerical evidence that initializing the level sets to have many small regions of positivity (or negativity) leads to a better segmentation.

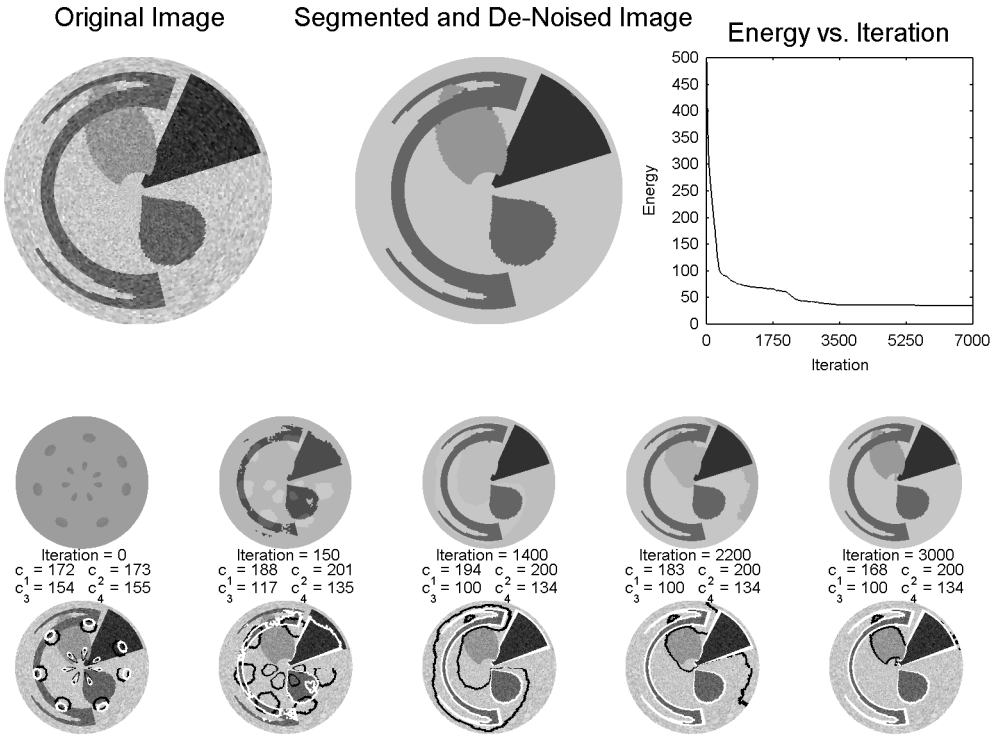

Figure 4. Segmentation using two level set functions. The original four color image is degraded by additive zero-mean Gaussian noise with standard deviation of 10 and RMSE=9.9158. The values for c_1, c_2, c_3, and c_4 in the original clean image are 100, 133, 167, and 200. In this example $\lambda = .1$ and $\mu = 1$. The recovered values for the constants are 100, 134, 167, and 200 (with RMSE=1.5719 for the denoised image). The four regions are recovered almost perfectly, with slight errors in the upper part of the image. The bottom five pairs of images show the evolution of the level set functions as well as the values of the coefficients at the given iteration.

3. SEGMENTATION OF MRI BRAIN DATA

Another application that we consider here is the segmentation of the 3D MRI brain data into three anatomical regions, called white matter (WM), gray matter (GM) and cerebro-spinal fluid (CSF). We assume that the data, provided by the Center for Computational Biology, UCLA, has been skull-stripped in advance. Our aim is to use again piecewise-constant segmentation based on the Chan-Vese models. Following[13] and,[14] we apply a multilayer level set approach: we use here two levels of the same level set function to represent the set of unknown boundaries. This gives an improved and more efficient model.

For this specific purpose, we first introduce an indicator function χ_B for the brain region denoted by B, obtained from the data, since we know that only the non-brain region has intensity value of zero. Then we segment only the brain region into three regions using two level lines of ϕ, given by $\{\phi = 0\}$ and $\{\phi = l\}$, with $l > 0$. The energy to be minimized becomes,

$$\begin{aligned} F(c_{GM}, c_{WM}, c_{CSF}, \phi) &= \int_\Omega |f(x) - c_{GM}|^2 \chi_B H(-\phi) dx + \int_\Omega |f(x) - c_{WM}|^2 \chi_B H(\phi) H(l - \phi) dx \\ &+ \int_\Omega |f(x) - c_{CSF}|^2 \chi_B H(\phi - l) dx + \mu \Big[length\{\phi = 0\} \cap B \\ &+ length\{\phi = l\} \cap B \Big]. \end{aligned}$$

The sum of the two length terms of contours inside B in the energy above is given by

$$\mu\Big[\int_\Omega \chi_B(x)\delta(\phi(x))|\nabla\phi(x)|dx + \int_\Omega \chi_B(x)\delta(\phi(x)-l)|\nabla\phi(x)|dx\Big].$$

Minimizing now the corresponding approximate energy F_ε using (6) alternately with respect to the unknowns, yields the associated Euler-Lagrange equations, parameterizing in the descent direction by an artificial time $t \geq 0$:

$$\phi(0,x) = \phi_0(x), \tag{11}$$

$$c_{GM}(t) = \frac{\int_\Omega f(x)H(-\phi(t,x))\chi_B(x)dx}{\int_\Omega H(-\phi(t,x))\chi_B(x)dx}, \tag{12}$$

$$c_{WM}(t) = \frac{\int_\Omega f(x)H(\phi(t,x))H(l-\phi(t,x))\chi_B(x)dx}{\int_\Omega H(\phi(t,x))H(l-\phi(t,x))\chi_B(x)dx}, \tag{13}$$

$$c_{CSF}(t) = \frac{\int_\Omega f(x)H(\phi(t,x)-l)\chi_B(x)dx}{\int_\Omega H(\phi(t,x)-l)\chi_B(x)dx}, \tag{14}$$

$$\frac{\partial\phi}{\partial t} = \delta_\varepsilon(\phi)\Big[|f-c_{GM}|^2\chi_B - |f-c_{WM}|^2\chi_B H(l-\phi) + \mu\mathrm{div}\Big(\chi_B\frac{\nabla\phi}{|\nabla\phi|}\Big)\Big] \tag{15}$$

$$+ \delta_\varepsilon(\phi-l)\Big[|f-c_{WM}|^2\chi_B H(\phi) - |f-c_{CSF}|^2\chi_B + \mu\mathrm{div}\Big(\chi_B\frac{\nabla\phi}{|\nabla\phi|}\Big)\Big].$$

(16)

In Figures 5 and 6, we illustrate a numerical result applied to real volumetric MRI data. We show particular 2D slices of the data and of the segmented results, together with the recovered surfaces, as boundaries of gray matter and white matter regions.

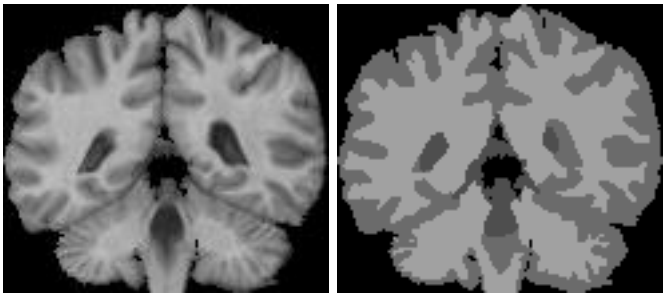

Figure 5. Left: 2D MRI slice, real data. Right: our proposed segmentation result.

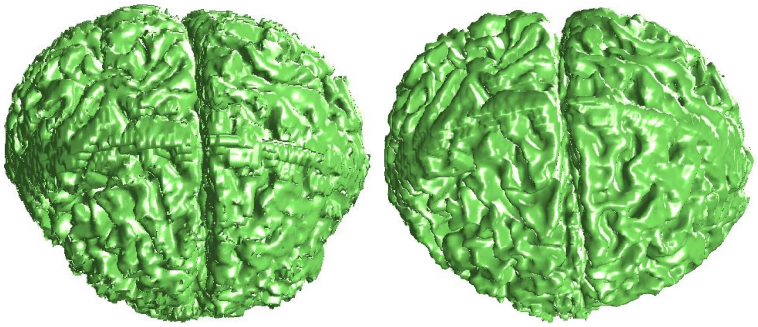

Figure 6. Boundaries of gray matter (left), and of white matter (right).

4. IMAGE RESTORATION AND DECOMPOSITION BY DUAL FUNCTIONALS

This section is devoted to new models for image restoration and image decomposition into cartoon and texture. The proposed models can be seen as refinements of the (BV, L^2) model of Rudin-Osher-Fatemi[2] by using better texture norms instead of the L^2 norm in the fidelity term.

In particular, inspired by Meyer,[15] we can view the R-O-F model (7) with $K = I$ as an image decomposition of f into $u + v$, with u a function of bounded variation (i.e. $\int_\Omega |\nabla u| < \infty$) and $v = f - u \in L^2(\Omega)$ an oscillatory residual of zero mean, representing texture or noise:

$$\inf_{u,v} \Big\{ E^{ROF}(u, v) = \int_\Omega |\nabla u| + \lambda \int_\Omega |f - u|^2 dx, \quad f = u + v \Big\}.$$

We call u the cartoon or geometric component of f, since it is a simplified version of the data, and v is called the oscillatory component.

Chan-Strong,[16] Meyer[15] and others have remarked that the R-O-F model does not always give the desired result. Indeed, if for instance f is the characteristic function of some smooth convex domain (circle), then we would like to obtain $f = u$. However this does not hold, for any coefficient λ. The residual v always attracts a small BV component. There is too much constraint on the minimizers u and $v = f - u$. To overcome this, we have to consider weaker norms. One way is to use non-convex and sub-linear potentials of the form $\int_\Omega \phi(|\nabla u|)dx$ for u instead of the total variation. Another way, as proposed by Meyer,[15] is to keep the total variation as regularization in u and to substitute the L^2 norm of v by a weaker, more refined texture norm.

Y. Meyer suggested the use of duality (such as (BV, BV^*) models) to obtain weaker norms to represent the oscillatory component $v = f - u$. We propose here minimization models of the form $\inf_u \Phi(u) + \lambda \Phi^*(f - Ku)$, where K is a linear blur. We will consider in particular the penalty $u \in BV(\Omega)$, or more generally of the form $\int_\Omega \phi(|\nabla u|)dx < \infty$, with ϕ convex and of linear growth, as well as non-convex potentials. In the convex case these include the total variation minimization proposed by L. Rudin, S. Osher, and E. Fatemi.[2] Related recent work is proposed by J.-F. Aujol and A. Chambolle,[17] and by S. Levine,[18] where the authors use the duality given by the Legendre-Fenchel transform to solve cartoon and texture decomposition models. However, our approach proposed here is different.

In Vese-Osher,[19] ,[20] Osher-Sole-Vese,[21] Aujol and collaborators,[22] ,[23] approximations to the (BV, BV^*) model of Y. Meyer have been previously proposed.

The use of the dual norm of the total variation has also appeared, independently and contemporaneously, in S. Kindermann, S. Osher, and J. Xu's work[24] in a different framework.

In the context of modeling oscillatory components by generalized functions, we refer to Y. Meyer,[15] D. Mumford and B. Gidas,[25] and to,[19] ,[20] .[21] Recently, in Le-Vese,[26] the authors propose practical methods for solving approximations to Y. Meyer's $(BV, div(BMO))$ decomposition model, while in Lieu-Vese,[27] the authors generalize the models,[19] ,[20] ,[21] by proposing a (BV, H^{-s}) decomposition model and theoretical results based on duality.

For more properties and notations regarding characterization of minimizers by duality for the Rudin-Osher-Fatemi model, we refer to[15] and.[28]

4.1. Description of the Model

Let E be a normed space, and let E^* be its dual space. Let $\Phi : E \to [0, \infty]$ be any function. Let us define $\Phi^* : E^* \to [0, \infty]$, by

$$\Phi^*(v) = \sup \Big\{ \frac{< v, u >}{\Phi(u)} : \ u \in E \Big\},$$

with the convention that $\frac{0}{0} = 0$, $\frac{0}{\infty} = 0$. Here, $< v, u >= v(u)$ denotes the duality pairing.

Note that $\Phi^*(v) \geq 0$, for any $v \in E^*$. Note also that the supremum is attained on the set of $u \in E$ such that $< v, u > \geq 0$. Note also that we have the following Cauchy-Schwartz inequality

$$< v, u > \leq \Phi^*(v)\Phi(u) \quad \text{if } \Phi(u) > 0.$$

Motivated by Meyer, we propose here image decomposition models of the form

$$\inf\Big\{\Phi(u)+\lambda\Phi^*(v),\ u\in E,\ v\in E^*,\ f=u+v\Big\}, \tag{17}$$

where $f\in E^*$ is a given data. The component u models the cartoon part of f, while the component v models the rough, oscillatory, or noise part of f. We will choose Φ so that if $\Phi(u)<\infty$, then u is a piecewise-smooth function, with homogeneous regions and sharp boundaries. In two dimensions, let us consider the particular case $E=L^2(\Omega)$, $E^*=E=L^2(\Omega)$, $<v,u>=\int_\Omega uvdx$, for $u,v\in L^2(\Omega)$, and

$$\Phi(u)=\begin{cases}\int_\Omega|\nabla u| \text{ if } u\in BV(\Omega),\\ +\infty \text{ if } u\in L^2(\Omega)\setminus BV(\Omega).\end{cases} \tag{18}$$

Let $X=\{v\in L^2(\Omega):\ \int_\Omega v(x)dx=0\}$. For $v\in X$, define

$$\|v\|_*:=\Phi^*(v)=\sup_{w\in BV(\Omega),|w|_{BV(\Omega)}\neq 0}\frac{\int_\Omega vwdx}{|w|_{BV(\Omega)}}=\sup_{w\in BV(\Omega),|w|_{BV(\Omega)}\neq 0}\frac{|\int_\Omega vwdx|}{|w|_{BV(\Omega)}}, \tag{19}$$

where $|w|_{BV(\Omega)}=\int_\Omega|\nabla w|$ is the total variation of $w\in BV(\Omega)$.

It is shown in[28] that

$$\Phi^*(v)=\inf\{\|\vec{g}\|_\infty:\ \vec{g}\in\Big(L^\infty(\Omega)\Big)^2,\ \mathrm{div}\vec{g}\in L^2(\Omega),\ v=-\mathrm{div}(\vec{g})\text{ in }\mathcal{D}'(\Omega),\ [\vec{g},\nu]=0\},$$

where ν denotes the outward unit normal to $\partial\Omega$ and $[g,\nu]$ is the trace of the normal component of g.

Since at every pixel the light intensity has finite energy, we can assume that $f\in L^\infty(\Omega)\subset L^2(\Omega)$ since Ω is bounded. Therefore, it is not too restrictive to assume that $f\in L^2(\Omega)$. We are interested in decomposing f into $u+v$, with $u\in BV(\Omega)$ and $v:=f-u\in X$. The first term u corresponds to a cartoon component, while v corresponds to an additive oscillatory component of zero mean (such as additive noise or texture).

One of the minimization models that we would like to solve is, given $f\in L^2(\Omega)$,

$$\inf\{E(u,v)=|u|_{BV(\Omega)}+\lambda\|v\|_*,\ f=u+v,\ u\in BV(\Omega),\ v\in X\},$$

which is equivalent with

$$\inf_{u\in BV(\Omega)}E(u)=|u|_{BV(\Omega)}+\lambda\|f-u\|_*, \tag{20}$$

or again with (17) with Φ given by (18). We call this a (BV,BV^*) algorithm because $u\in BV(\Omega)$ while $v\in BV^*(\Omega)\cap L^2(\Omega)$.

4.1.1. (BV,BV^*) Minimization Algorithm

In the following formal calculations of Euler-Lagrange equations and in practice, we will use the notation $|u|_{BV(\Omega)}=\int_\Omega|\nabla u|dx$ for the total variation of u.

- Start with u^0.
- For integers $n\geq 0$, if u^n is known or previously computed, estimate w^n by the maximization process:

$$\|f-u^n\|_*\approx\sup_{w\in BV(\Omega),|w|_{BV(\Omega)}\neq 0}\frac{\int(f-u^n)wdx}{\int\sqrt{\epsilon^2+|\nabla w|^2}dx}.$$

The associated PDE in $w=w^n$, to obtain w^n, formally is

$$0=\frac{f-u^n}{\int_\Omega\sqrt{\epsilon^2+|\nabla w|^2}dx}+\frac{\int_\Omega(f-u^n)wdx}{(\int_\Omega\sqrt{\epsilon^2+|\nabla w|^2}dx)^2}\mathrm{div}\Big(\frac{\nabla w}{|\nabla w|}\Big), \tag{21}$$

or

$$0 = (f - u^n) + \frac{\int_\Omega (f - u^n) w dx}{\int_\Omega \sqrt{\epsilon^2 + |\nabla w|^2} dx} \mathrm{div}\Big(\frac{\nabla w}{|\nabla w|}\Big), \tag{22}$$

with natural boundary condition $\frac{\partial w}{\partial \nu} = 0$ on $\partial\Omega$.

- Once w^n is computed, then we compute u^{n+1} by minimizing with respect to $u = u^{n+1}$ the energy

$$E(u) = \int_\Omega |\nabla u| dx + \lambda \frac{\int_\Omega (f - u) w^n dx}{|w^n|_{BV(\Omega)}},$$

that formally gives the associated Euler-Lagrange equation in $u = u^{n+1}$:

$$0 = \frac{\lambda w}{|w|_{BV(\Omega)}} + \mathrm{div}\Big(\frac{\nabla u}{|\nabla u|}\Big), \tag{23}$$

or

$$0 = w + \frac{|w|_{BV(\Omega)}}{\lambda} \mathrm{div}\Big(\frac{\nabla u}{|\nabla u|}\Big), \tag{24}$$

with $\frac{\partial u}{\partial \nu} = 0$ on $\partial\Omega$.

As before, in a time-dependent approach, the main algorithm is summarized as follows: start with $(u^0, w^0) = (u(0,x), w(0,x))$, and solve for $t > 0$

$$\frac{\partial w}{\partial t} = f - u + \frac{\int_\Omega (f - u) w dx}{\int_\Omega \sqrt{\epsilon^2 + |\nabla w|^2} dx} \mathrm{div}\Big(\frac{\nabla w}{|\nabla w|}\Big), \tag{25}$$

$$\frac{\partial u}{\partial t} = w + \frac{|w|_{BV(\Omega)}}{\lambda} \mathrm{div}\Big(\frac{\nabla u}{|\nabla u|}\Big). \tag{26}$$

4.1.2. Deblurring Models

Note that the above model (20) can also be applied to image deblurring. Let $K : L^2(\Omega) \to L^2(\Omega)$ be a linear and continuous operator (sometimes, we have to assume in addition that K does not annihilate constants). If we assume the degradation model $f = Ku + n$, where K denotes a blurring operator and n denotes additive noise of zero mean, then we propose the following restoration model:

$$\inf_{u \in BV(\Omega)} E(u) = |u|_{BV(\Omega)} + \lambda \|f - Ku\|_*, \tag{27}$$

or

$$\inf_{u \in BV(\Omega)} E(u) = \Phi(u) + \lambda \Phi^*(f - Ku), \tag{28}$$

with Φ defined in (18). We apply the same steps in the minimization algorithm as before, and the associated time-dependent Euler-Lagrange equations formally are:

$$\frac{\partial w}{\partial t} = \frac{f - Ku}{\int_\Omega \sqrt{\epsilon^2 + |\nabla w|^2} dx} + \frac{\int_\Omega (f - Ku) w dx}{(\int_\Omega \sqrt{\epsilon^2 + |\nabla w|^2} dx)^2} \mathrm{div}\Big(\frac{\nabla w}{|\nabla w|}\Big), \tag{29}$$

$$\frac{\partial u}{\partial t} = \frac{\lambda K^* w}{|w|_{BV(\Omega)}} + \mathrm{div}\Big(\frac{\nabla u}{|\nabla u|}\Big), \tag{30}$$

where K^* denotes the adjoint operator of K. Note that here we no longer have to invert K^*Ku. In the R-O model[12] with the fidelity term $\|f - Ku\|^2_{L^2(\Omega)}$, the operator K^*Ku has to be inverted at each iteration.

4.1.3. General (Φ, Φ^*) Decomposition Model

Similarly, consider a general decomposition model of the form (17), or

$$\inf_u \Big\{ \int_\Omega \phi(|\nabla u|)\ dx + \lambda \sup_{w, \int_\Omega \phi(|\nabla w|)dx \neq 0} \frac{\int_\Omega (f-u)w\ dx}{\int_\Omega \phi(|\nabla w|)\ dx} \Big\}. \tag{31}$$

We assume that ϕ is a differentiable, increasing function on $[0,\infty)$, possibly non-convex, with at most linear growth at infinity, and satisfying $\phi(0) > 0$ again to avoid division by zero. In the convex case, the measure $\int_\Omega \phi(|\nabla u|)$ is well defined for $u \in BV(\Omega)$. In the non-convex case, we work with $u \in W^{1,1}(\Omega) \subset BV(\Omega) \subset L^2(\Omega)$ and the distributional gradient ∇u as a function in $(L^1(\Omega))^2$.

In the same way, to minimize this functional, we solve an evolutionary coupled system in the unknowns u, w as follows:

$$\frac{\partial w}{\partial t} = f - u + \frac{\int_\Omega (f-u)w dx}{\int_\Omega \phi(|\nabla w|)dx} \mathrm{div}\Big(\phi'(|\nabla w|)\frac{\nabla w}{|\nabla w|}\Big), \tag{32}$$

$$\frac{\partial u}{\partial t} = w + \frac{|w|_{BV(\Omega)}}{\lambda} \mathrm{div}\Big(\phi'(|\nabla u|)\frac{\nabla u}{|\nabla u|}\Big). \tag{33}$$

4.1.4. Experimental Results

We show in Figure 7 a decomposition result of a real fingerprint image into its cartoon and oscillatory components using the (BV, BV^*) proposed decomposition model.

Figure 7. Exact image decomposition into cartoon and texture using the (BV, BV^*) minimization model. Left: real fingerprint data. Middle: cartoon component u. Right: oscillatory component $v = f - u$ (+125).

We apply next the deblurring model proposed in (27), and solved using the coupled system (29)-(30). The blur operator Ku is given by a convolution with a 5×5 blurring mask or kernel k of the form:

$$\frac{1}{273} \cdot \begin{array}{|c|c|c|c|c|} \hline 1 & 4 & 7 & 4 & 1 \\ \hline 4 & 16 & 26 & 16 & 4 \\ \hline 7 & 26 & 41 & 26 & 7 \\ \hline 4 & 16 & 26 & 16 & 4 \\ \hline 1 & 4 & 7 & 4 & 1 \\ \hline \end{array}$$

We can see in Figure 8 an experimental result of image deblurring.

We end the paper with two experimental results of denoising using a non-convex potential $\phi(t) = \frac{|t|^q}{1+\alpha|t|^q}$ in (31), with $\alpha = 0.001$ and $q = 2$. In Figure 9 we apply the model to a synthetic noisy image, while in Figure 10

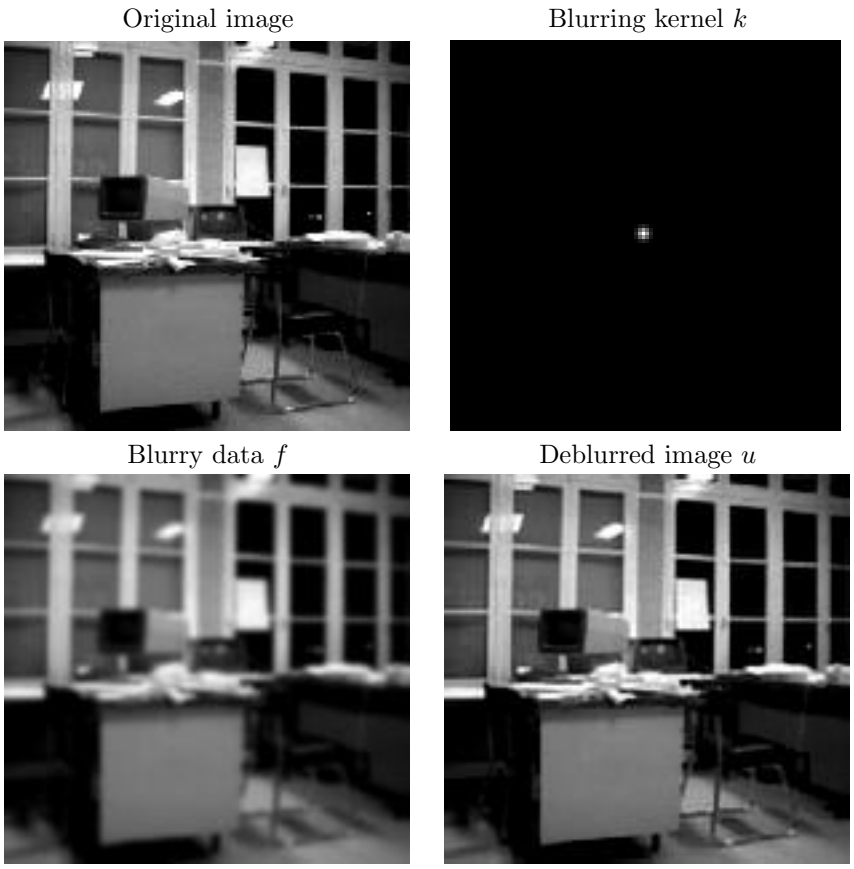

Figure 8. Image deblurring using the (BV, BV^*) decomposition model with blur. Top: original image of an office (left), a blurring kernel (right). Bottom: blurry data f, restored image u.

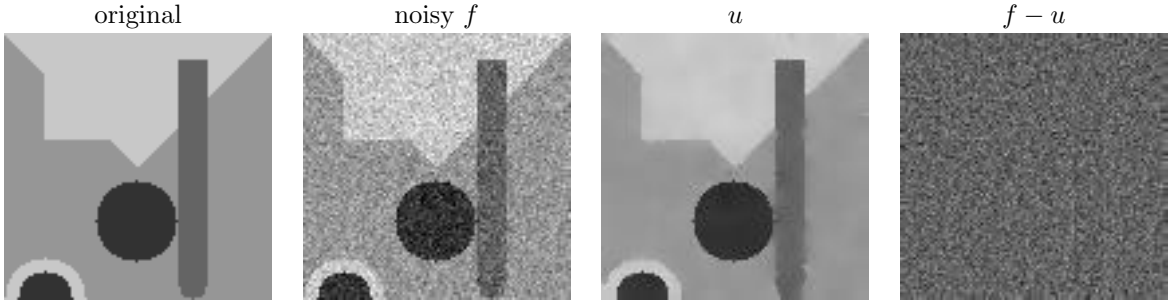

Figure 9. Image denoising using a non-convex potential and duality. $RMSE = 0.05111486$, $\lambda = 8$.

we consider a real noisy image. In both cases, we also show the residual term $v = f - u$, and note that there is not much geometry left in v.

For references to non-convex regularizing terms $\int_\Omega \phi(|\nabla u|)dx$ in anisotropic image smoothing we refer the reader for example to Geman and Reynolds,[29] among other work. For more details and results on the proposed dual models, we refer the reader to.[30]

Figure 10. Image denoising using a non-convex potential and duality. $RMSE = 0.02260758$, $\lambda = 5$.

ACKNOWLEDGMENTS

L.A.V. would like to thank the editors Charles A. Bouman, Eric L. Miller, and Ilya Pollak for their kind invitation to speak in the SPIE Conference "Computational Imaging IV", San Jose, CA, January 2006.

This work has been supported in part by an Alfred P. Sloan fellowship (L.A.V.), by the National Institute of Health through the NIH Roadmap for Medical Research (Grant U54 RR021813 entitled Center for Computational Biology CCB), by the National Science Foundation Grants NSF ITR 0113439, NSF DMS 0312222, NSF Vigre DMS-0502315 (N.M.T.), by a UC Dissertation Year Fellowship (T.M.L.), and by the IPAM Institute for Pure and Applied Mathematics (T.M.L. and G.C.).

REFERENCES

1. D. Mumford and J. Shah, "Optimal approximations by piecewise smooth functions and variational problems," *Communications on Pure and Applied Mathematics* **XLII**(5), pp. 577–685, 1988.
2. L. Rudin, S. Osher, and E. Fatemi, "Nonlinear total variation based noise removal algorithms," *Physica D: Nonlinear Phenomena* **60(1-4)**, pp. 259–268, 1992.
3. T. F. Chan and L. A. Vese, "An active contour model without edges," in *Scale-Space Theories in Computer Vision, Lecture Notes in Computer Science*, **1682**, pp. 141–151, 1999.
4. T. F. Chan and L. A. Vese, "Active contours without edges," *IEEE Trans. Image Processing* **10(2)**, pp. 266–277, 2001.

5. T. F. Chan and L. A. Vese, "A level set algorithm for minimizing the mumford-shah functional in image processing," in *IEEE Workshop on Variational and Level Set Methods in Computer Vision*, pp. 161–168, 2001.
6. L. A. Vese and T. F. Chan, "A multiphase level set framework for image segmentation using the mumford and shah model," *International Journal of Computer Vision* **50**(3), pp. 271–293, 2002.
7. L. Ambrosio and V. Tortorelli, "Approximation of functionals depending on jumps by elliptic functionals via gamma-convergence," *C.P.A.M.* **43 (8)**, pp. 999–1036, 1990.
8. L. Ambrosio and V. Tortorelli, "On the approximation of free discontinuity problems," *Bollettino della Unione Matematica Italiana* **6B (1)**, pp. 105–123, 1992.
9. G. Koepfler, C. Lopez, and J. M. Morel, "A multiscale algorithm for image segmentation by variational method," *SIAM J. of Numerical Analysis* **31**(1), pp. 282–299, 1994.
10. A. Tsai, A. J. Yezzi, Jr., and A. S. Willsky, "Curve evolution implementation of the mumford-shah functional for image segmentation, denoising, interpolation, and magnification," *IEEE Trans. Image Processing* **10**(8), pp. 1169–1186, 2001.
11. H. Zhao, T. Chan, B. Merriman, and S. Osher, "Variational level set approach to multiphase motion," *JCP* **127 (1)**, pp. 179–195, 1996.
12. L. I. Rudin and S. Osher, "Total variation based image restoration with free local constraints," in *ICIP (1)*, pp. 31–35, 1994.
13. G. Chung and L.A.Vese, "Energy minimization based segmentation and denoising using a multilayer level set approach," in *LNCS*, **3757**, pp. 439 – 455, 2005.
14. G. Chung and L. Vese, "Image segmentation using a multilayer level-set approach," *UCLA CAM Report* (03-53), 2003.
15. Y. Meyer, *Oscillating Patterns in Image Processing and Nonlinear Evolution Equations*, Volume 22, AMS, 2001.
16. D. Strong and T. Chan, "Edge-preserving and scale-dependent properties of total variation regularization," *Inverse Problems* **19 (6)**, pp. S165–S187, 2003.
17. J.-F. Aujol and A. Chambolle, "Dual norms and image decomposition models," *IJCV* **3(1)**, pp. 85–104, 2005.
18. S. Levine, "An adaptive variational model for image decomposition," in *LNCS*, **3757**, pp. 382–397, 2005.
19. L. Vese and S. Osher, "Modeling textures with total variation minimization and oscillating patterns in image processing," *Journal of Scientific Computing* **19(1-3)**, pp. 553–572, 2003.
20. L. A. Vese and S. J. Osher, "Image denoising and decomposition with total variation minimization and oscillatory functions," *Journal of Mathematical Imaging and Vision* **20**(1-2), pp. 7–18, 2004.
21. S. J. Osher, A. Solé, and L. A. Vese, "Image decomposition, image restoration, and texture modeling using total variation minimization and the H^{-1} norm," in *International Conference on Image Processing*, pp. I: 689–692, 2003.
22. J.-F. Aujol, G. Aubert, L. Blanc-Féraud, and A. Chambolle, "Image decomposition application to SAR images," in *Scale-Space*, pp. 297–312, 2003.
23. J. F. Aujol, G. Aubert, L. Blanc-Féraud, and A. Chambolle, "Image decomposition into a bounded variation component and an oscillating component," *Journal of Mathematical Imaging and Vision* **22**, pp. 71–88, Jan. 2005.
24. S. Kindermann, S. Osher, and J. Xu, "Denoising by bv-duality," *UCLA CAM Report* (05-21), 2005.
25. B. Mumford, D. Gidas, "Stochastic models for generic images," *Quart. Appl. Math.* **59**, pp. 85–111, 2001.
26. T. Le and L. Vese, "Image decomposition using total variation and div(bmo)," *Multiscale Modeling and Simulation* **4(2)**, pp. 390–423, 2005.
27. L. Lieu and L. Vese, "Image restoration and decomposition via bounded total variation and negative hilbert-sobolev spaces," *UCLA CAM Report* (05-33), 2005.
28. F. Andreu-Vaillo, V. Caselles, and J. Mazon, *Parabolic Quasilinear Equations Minimizing Linear Growth Functionals*, Progress in Mathematics Vol. 223, Birkhauser, 2004.
29. D. Geman and G. Reynolds, "Constrained restoration and the recovery of discontinuities," *IEEE T. on PAMI* **14 (3)**, pp. 367–383, 1992.

30. T. M. Le, L. H. Lieu, and L. A. Vese, "Bv and dual of bv image decomposition models and minimization algorithms," *UCLA CAM Report* (05-13), 2005.